Received June 11, 2020, accepted June 25, 2020, date of publication July 13, 2020, date of current version July 22, 2020.

Digital Object Identifier 10.1109/ACCESS.2020.3006157

The Remaining Useful Life Prediction by Using Electrochemical Model in the Particle Filter Framework for Lithium-Ion Batteries

QIANQIAN LIU[1], JINGYUAN ZHANG[1], KE LI[1], AND CHAO LV[2], (Senior Member, IEEE)

[1]Naval University of Engineering, Wuhan 430033, China
[2]School of Electrical Engineering and Automation, Harbin Institute of Technology, Harbin 150001, China

Corresponding author: Qianqian Liu (liuhe1984@163.com)

ABSTRACT The remaining useful life (RUL) prediction is critical for the safe and reliable operation of lithium-ion battery (LIB) systems, which characterizes the aging status of the battery and provides early warning for battery replacement. Most existing RUL prediction methods rely on empirical aging models, and the role of the battery mechanism is not considered in the subsequent algorithm settings. The accuracy and stability of data-driven algorithms are severely limited by battery aging data. A new electrochemical-model-based particle filter (PF) framework for LIB RUL prediction is proposed in this paper. Parameters of a simplified electrochemical model (SEM) are used as state variables of the PF algorithm and these parameters can be identified by applying specially designed current excitations to the battery. The SEM-based capacity simulation process is taken as the observation equation in the PF algorithm framework. Therefore, the mechanism of the battery is fully considered when making the RUL prediction. The proposed method is validated through cyclic aging experiment of a cylindrical LFP/graphite LIB of 45Ah. The accuracy of the method is compared with a data-driven-based PF framework for RUL prediction and shows better accuracy and stability, which provides a choice for achieving high-quality RUL prediction.

INDEX TERMS Lithium ion battery, new particle filter framework, simplified electrochemical model, remaining useful life prediction.

I. INTRODUCTION

LIBs are widely used in many energy storage applications because of their high energy density, high power density, and high charge/discharge rate [1]. However, LIBs suffer from the problem of aging, i.e., capacity fades with cycles and time. Moreover, LIBs in service may fail to supply the needed energy that leads to the whole system's breakdown. A battery's RUL is usually defined as the number of cycles the battery can be recharged before its capacity has faded beyond acceptable limits (typically 20%) [2]. The RUL represents the battery degradation state and alerts when the battery should be substituted. Accurate prediction of RUL is of great significance for the management of state of health (SOH) of LIBs.

The capacity of LIB is usually used as direct health indicator for RUL prediction. Nuhic *et al.* [3] simulated the capacity degradation behavior and predicted RUL based on support vector regression (SVR) which is another name for support vector machine (SVM) when it is used as a regression analysis tool. Qin *et al.* [4] further optimized the kernel parameters of SVR by using particle swarm optimization (PSO) and improved SVR-based RUL prediction. Li *et al.* [5] introduced a novel prediction method based on the Gaussian Process Mixture (GPM) to simulate the multimodality of capacity degeneration trajectories in the LIB RUL estimation. Long *et al.* [6] improved the autoregressive (AR) model for capacity fading by using PSO to search the optimal AR model order. Ma *et al.* [7] proposed a hybrid neural network with the false nearest neighbor method to resolve the unreliable sliding window sizes in data-driven RUL prediction algorithm. Zhang *et al.* [8] showed that the long short-term memory (LSTM) recurrent neural network (RNN) can be employed to simulate the long-term dependencies of the degraded LIBs capacities and can be used as a RUL predictor after training.

The associate editor coordinating the review of this manuscript and approving it for publication was Reinaldo Tonkoski.

There are LIB RUL predictions use indirect health characteristics (HCs) derived from battery's terminal voltage, load current and capacity to reflect LIB degradation. Li *et al.* [9] used the sample entropy of cell voltage in urban dynamometer driving schedule (UDDS) conditions as the HC relating to LIBs SOH. Guo *et al.* [10] adopted an adaptive transformation of charging curves at different stages of life to quantify the extent of capacity fade and derived a time-based parameter to enable an accurate SOH estimation by fitting an equivalent circuit model (ECM). Li *et al.* [11] used the incremental capacity analysis (ICA) to reveal the aging mechanism of NMC batteries and found out a linear regression relationship between the positions of peaks in IC curves (incremental capacity vs. terminal voltage curve) with cycles and capacity. Differential thermal voltammetry (DTV) analysis was carried out to estimate SOH as diagnostic techniques, which combined ICA to reflect thermodynamic information about the electrode materials. Maher and Yazami [12] observed that the DTV profiles of aged cells show variation in peak positions and amplitudes which are similar to those displayed by IC profiles. Li *et al.* [13] fitted an ECM to the measured electrochemical impedance spectrum (EIS). The 10 parameters of the ECM were selected as SOH indicators for the battery degradation.

Adaptive filter algorithms are often used for LIB RUL prediction. Zheng and Fang [14] used the unscented Kalman filter (UKF) to recursively estimate the battery degradation model parameters for predicting RUL. Miao *et al.* [15] completed the RUL prediction based on the unscented particle filter (UPF) by adjusting the parameters of double exponential capacity degradation model. Saha *et al.* [16] proposed a method to predict LIBs RUL based on the slope of the charge voltage curve. In J. Hoo's study, uncertainties were minimized by a Bayesian framework and a PF algorithm was applied to predict the RUL in the form of a probability distribution function (PDF).

The existing LIB RUL predictions estimate the tendency of degradation as a time series. On one hand, the empirical models or networks are fitted or trained through historical data, neglecting that the objects studied are batteries. On the other hand, the relationships between SOH indicators and capacity are also data-driven, which rely on working conditions of battery (load profile, ambient temperature, etc.). To add more battery's mechanism information to RUL prediction methods is a potential resolution to push forward this technology.

Our previous work, reference [2], introduces a PF-based RUL prediction framework for lead-acid batteries by incorporating the physics of working and aging of the batteries through a full-order electrochemical model. However, applying this roadmap to the RUL prediction for lithium-ion batteries needs to be verified and faces challenges. Firstly, the electrochemical model for lithium-ion batteries used in the framework should be a compromise between accuracy and complexity to meet the requirements of accrual applications. Secondly, a robust parameterization method is needed to avoid local optimal problem of genetic algorithm used in reference [2].

A novel physics-based RUL prediction method for LIBs is shown in this paper. A simplified electrochemical model for lithium-ion battery is integrated into the PF-based RUL prediction framework for better robustness and accuracy. The advantage of this method is that when the PF is updated iteratively, the aging and working mechanisms of the LIBs are considered as well. The rest of this paper follows as: in Section II, a simplified electrochemical model of LIBs is introduced based on the previous work by Lyu *et al.* [17]; in Section VI, parameters of this model are identified by means of excitation-and-response method and the simulation accuracy of this model is verified as well; in Section VI, an electrochemical-model-based PF framework is introduced, the effectiveness of which is validated through actual aging experiment.

II. SIMPLIFIED ELECTROCHEMICAL MODEL FOR LITHIUM-ION BATTERY

The simplified electrochemical model (SEM) of LIBs is a reduced order version of the well-known P2D model [17]. The simplification has four main aspects. First, the effect of uneven reaction distribution is ignored and multiple active particles in the positive and negative electrodes are taken as single particle. Second, the distribution of the ion concentration in the active particles in the radius r direction is approximated by using a three-parameter parabola. Third, the distribution of the ion concentration in the electrolyte in the thickness l direction is solved by using another three-parameter parabolic approximation. Finally, the distribution of the ion concentration in the separator in the l direction is solved by a linear approximation. Fig. 1. shows the structure of the SEM. The factors that affect the battery terminal voltage are the open circuit voltage, E_{ocv}, ohmic overpotential, $\eta_{ohm,}$ reaction overpotential, η_{act}, and concentration overpotential, η_{con}.

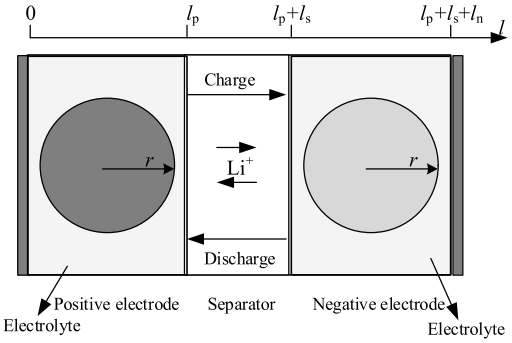

FIGURE 1. Schematic diagram of the SEM.

The first factor is the open circuit voltage of the battery. The open circuit voltage of the battery, E_{ocv}, is determined by the ion intercalation concentration of both the positive and negative active materials, the calculation of which is shown

in Eq. (1).

$$E_{\mathrm{ocv}}(t) = U_{\mathrm{p}}(y_{\mathrm{surf}}(t)) - U_{\mathrm{n}}(x_{\mathrm{surf}}(t)) \tag{1}$$

where, U_p and U_n represent positive and negative electrode open circuit voltage, respectively. Variables y_{surf} and x_{surf} are solid-phase surface stoichiometric number for positive and negative electrodes, respectively.

The solid-phase surface stoichiometric numbers of the positive and negative electrodes are calculated from the solid-phase average stoichiometric number, as shown in Eq. (2).

$$\begin{cases} y_{\mathrm{surf}}(t) = y_{\mathrm{avg}}(t) + \Delta y(t) \\ x_{\mathrm{surf}}(t) = x_{\mathrm{avg}}(t) - \Delta x(t) \end{cases} \tag{2}$$

where, y_{avg} and x_{avg} are the solid-phase average stoichiometric number of the positive and negative electrodes, respectively. And Δy is the difference between y_{surf} and y_{avg}. Variable Δx is the difference between x_{surf} and x_{avg}.

According to the approximation of the three-parameter parabola of the lithium ion concentration distribution in the active particles, variables Δy and Δx can be obtained by Eq.(3).

$$\begin{aligned} \Delta y(t) &= \Delta y'(t) + \frac{2}{7}\frac{\tau_{\mathrm{p}}}{Q_{\mathrm{p}}} \cdot I(t) \\ \Delta x(t) &= \Delta x'(t) + \frac{2}{7}\frac{\tau_{\mathrm{n}}}{Q_{\mathrm{n}}} \cdot I(t) \end{aligned} \tag{3}$$

where, $\Delta y'$ and $\Delta x'$ are the intermediate variables, and τ_p and τ_n are the solid-phase diffusion time constants of the positive and negative electrodes, respectively.

The calculation formulas of $\Delta y'$ and $\Delta x'$ are as follows by discretizing formula (3).

$$\begin{cases} \Delta y'(t_{k+1}) = \Delta y'(t_k) + \frac{1}{\tau_s^{\mathrm{p}}}(\frac{12}{7}\frac{\tau_{\mathrm{p}}}{Q_p} I(t_k) \\ \qquad\qquad -\Delta y'(t_k))(t_{k+1} - t_k) \\ \Delta x'(t_{k+1}) = \Delta x'(t_k) + \frac{1}{\tau_s^{\mathrm{n}}}(\frac{12}{7}\frac{\tau_{\mathrm{n}}}{Q_n} I(t_k) \\ \qquad\qquad -\Delta x'(t_k))(t_{k+1} - t_k) \end{cases} \tag{4}$$

The ohmic effect of each part of the battery can be expressed by a lumped ohmic resistance, R_{ohm}. The calculation of the ohmic overpotential, η_{ohm}, is as follows.

$$\eta_{\mathrm{ohm}}(t) = R_{\mathrm{ohm}} I(t) \tag{5}$$

On the premise of uniform reaction distribution, the reaction overpotential, η_{act}, can be calculated by the Bulter-Volmer equation.

$$\begin{cases} \eta_{\mathrm{act}}(t) = \frac{2RT}{F}(\ln(\sqrt{m_{\mathrm{n}}^2(t)+1} + m_{\mathrm{n}}(t)) \\ \qquad\qquad + \ln(\sqrt{m_{\mathrm{p}}^2(t)+1} + m_{\mathrm{p}}(t))) \\ m_{\mathrm{p}}(t) = \frac{1}{6Q_{\mathrm{p}}c_0^{0.5}} \frac{1}{(1-y_{\mathrm{surf}}(t))^{0.5}(y_{\mathrm{surf}}(t))^{0.5}} P_{\mathrm{act}} I(t) \\ m_{\mathrm{n}}(t) = \frac{1}{6Q_{\mathrm{n}}c_0^{0.5}} \frac{1}{(1-x_{\mathrm{surf}}(t))^{0.5}(x_{\mathrm{surf}}(t))^{0.5}} P_{\mathrm{act}} I(t) \end{cases} \tag{6}$$

where, R is the ideal gas constant. T is the ambient temperature. m_{n} and m_{p} are the intermediate calculation variables. F is the Faraday constant. P_{act} is the reaction polarization constant.

By using the three-parameter parabolic approximation of the lithium-ion concentration in the liquid phase, a formula for calculating the concentration overpotential, η_{con}, is obtained.

$$\eta_{\mathrm{con}}(t) = \frac{2RT}{F}(1-t_+)\ln(\frac{c_0 + \Delta c(t)}{c_0 - \Delta c(t)}) \tag{7}$$

where, c_0 is the initial electrolyte concentration. Δc is electrolyte concentration deviation from c_0 at the boundaries of both current collectors.

The discrete iteration formula for Δc is shown in Eq.(8).

$$\Delta c(t_{k+1}) = \Delta c(t_k) + \frac{1}{\tau_e}(P_{\mathrm{con}} I(t_k) - \Delta(t_k))(t_{k+1} - t_k) \tag{8}$$

where, τ_e is the liquid-phase diffusion time constant. P_{con} is the proportional coefficient of liquid-phase diffusion.

Based on the E_{ocv} and the aforementioned overpotentials, the battery terminal voltage, U_{app}, is determined by Eq.(9).

$$U_{\mathrm{app}}(t) = E_{\mathrm{ocv}}(t) - \eta_{\mathrm{con}}(t) - \eta_{\mathrm{act}}(t) - \eta_{\mathrm{ohm}}(t) \tag{9}$$

The parameters used in the SEM are summarized in table 1.

III. PARAMETER IDENTIFICATION AND MODEL VALIDATION

The LIBs used in this paper are cylindrical graphite/$LiFePO_4$ batteries with a rated capacity of 45 Ah. In order to avoid the influence of temperature on the model parameters, the parameter identification experiments were completed in a 25 °C incubator.

The battery terminal voltage is jointly determined by various mechanism processes. The basic working process, reaction polarization, concentration polarization, ohmic polarization, and the diffusion process of the positive and negative electrodes all have effects on the battery terminal voltage. The key to non-destructive parameter identification is to decouple the effects of various mechanism processes on the terminal voltage. The excitation and response method is to achieve the decoupling of each mechanism process through special charging and discharging operating conditions. According to the SEM description, the parameters identification process can be divided into the following five parts.

The first is the parameter identification of the basic working process. The basic working process is a process in which lithium ions insert and extract between the positive and negative electrodes as the battery is charged and discharged. For the identification of basic working process parameters, a small-rate discharge is used. The parameters describing this part mainly include y_{ofs}, y_0, Q_{p}, Q_{n}. When the battery is discharged at a small rate of 1/50C, the effects of the other mechanisms on the battery terminal voltage can be ignored. It can be approximated that the terminal voltage is the

TABLE 1. Parameter list of the SEM.

Parameter	Name [unit]	Descriptions
y_0	initial stoichiometric number of positive electrode [−]	Initial state of charge of positive electrode when battery is fully charged
Q_p	capacity of positive electrode [C]	Total operative active material in positive electrode
Q_n	capacity of negative electrode [C]	Total operative active material in negative electrode
y_{ofs}	offset in stoichiometric number [−]	Lithium-ions that exist in the active material but have difficulty in participating in electromigration and diffusion
τ_p	solid phase diffusion time constant of positive electrode [s]	Rate of solid phase diffusion of lithium-ions in positive electrode
τ_n	solid phase diffusion time constant of negative electrode [s]	Rate of solid phase diffusion of lithium-ions in negative electrode
P_{con}	proportional coefficient of liquid phase diffusion [mol/(m^3·A)]	Variation of lithium-ion concentration at the boundaries of current collectors
τ_e	liquid phase diffusion time constant [s]	Rate of liquid phase diffusion of lithium-ions
P_{act}	unified coefficient of activation polarization of the electrode [mol$^{0.5}$·s/m$^{1.5}$]	Rate of electrochemical reaction
R_{ohm}	ohmic resistance [Ω]	Ohmic polarization

open circuit voltage. Assuming that the surface and average concentrations of lithium-ions in the solid-phase particles are equal at small rate discharge condition, the terminal voltage can be derived from Eq. (1):

$$\begin{aligned} U_{app} &\approx E_{ocv} = U_p\left(y_{avg}\right) - U_n\left(x_{avg}\right) \\ &= U_p\left(y_{avg}\right) - U_n\left(\left(1 - y_{ofs} - y_{avg}\right) \cdot \frac{Q_p}{Q_n}\right) \end{aligned} \quad (10)$$

$$y_{avg} = y_0 + \frac{I \cdot t}{Q_p} \quad (11)$$

The relevant parameters of the basic working process can be obtained by performing a nonlinear least square fitting according to Eq. (9).

The parameters corresponding to the remaining four parts can be divided into a fast response process and a slow process according to the response time constant. Among them, the time constant of ohmic polarization and reaction polarization is short (about 10^{-2} seconds), which belongs to the fast response process, and the time constant of solid phase diffusion and liquid phase diffusion is long (about 10^2 seconds), which belongs to the slow response process.

Next, the parameters of the fast response process are identified. The operating condition for parameter identification of this part is instantaneous pulse current. As shown in Fig. 2, the fast change of voltage is caused by reactive polarization and ohmic polarization when the current is abrupt. The ohmic internal resistance constant, R_{ohm} of ohmic polarization can be measured by an ohmic resistance tester. Therefore, the electromotive force generated by reactive polarization can be calculated by using formula (12).

$$\eta_{act} = \eta_{fast} - \eta_{ohm} \quad (12)$$

Combined with the calculation formula of η_{act} in formula (6) and using the nonlinear least squares fitting method, the reactive polarization constant P_{act} can be obtained.

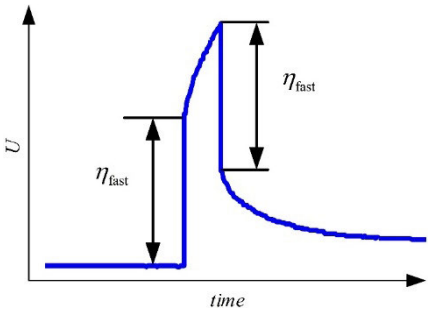

FIGURE 2. Terminal voltage vs. time during current interruption.

Next, the parameter identification of the slow response process is performed. The slow response process is caused by solid-phase diffusion and liquid-phase diffusion. According to electrochemical knowledge, the time constant of the solid-phase diffusion process is longer than the time constant of the liquid-phase diffusion process. The decoupling of these two parts can be achieved through constant current discharge with different time length.

After a long time (more than 10^3 seconds) constant current discharge, the diffusion process inside the battery has stabilized. At this moment, the terminal voltage calculation formula of the battery is formula (13).

$$U_{app}(t) = E_{ocv}^{stable}(t) - \eta_{con}^{stable}(t) - \eta_{act}(t) - \eta_{ohm}(t) \quad (13)$$

where, E_{ocv}^{stable} is the steady-state open circuit voltage, and η_{con}^{stable} is the steady-state concentration polarization overpotential. The calculation formula of E_{ocv}^{stable} is as follows.

$$\begin{cases} E_{ocv}^{stable}(t) = U_p(y_0(t) + \Delta y^{stable}) - U_n(x_0(t) - \Delta x^{stable}) \\ \Delta y^{stable} = 2\dfrac{\tau_p^s}{Q_p} \cdot I,\ \Delta x^{stable} = 2\dfrac{\tau_n^s}{Q_n} \cdot I \end{cases} \quad (14)$$

Substituting formula (14) into formula (13), where the reactive polarization overpotential, η_{act}, and the ohmic polarization overpotential, η_{ohm}, can be obtained directly. Δy^{stable}, Δx^{stable}, and, η_{con}^{stable} are obtained by nonlinear least squares fitting. Based on Δy^{stable} and Δx^{stable}, the solid-phase diffusion time constants, τ_p and τ_n, of the positive and negative electrodes can be directly obtained, and the liquid phase diffusion coefficient P_{con} can be obtained by inversely solving formula (7) and formula (8).

Finally, only the liquid-phase diffusion time constant remains to be identified. The short-term (10^2 seconds) constant current discharge can be used to complete the identification of liquid-phase diffusion time constant. Based on the parameters identified above, the concentration polarization overpotential η_{con} can be obtained directly using formula (15).

$$\eta_{con}(t) = E_{ocv}(t) - U_{app}(t) - \eta_{act}(t) - \eta_{ohm}(t) \quad (15)$$

From η_{con}, the difference in liquid phase lithium ion concentration, Δc, between the boundary of the positive and negative electrode current collectors can be obtained, as shown in formula (16).

$$\Delta c(t) = c_0 \frac{\exp(\eta_{con} F/(2RT(t)(1-t_+))) - 1}{\exp(\eta_{con} F/(2RT(t)(1-t_+))) + 1} \quad (16)$$

Finally, from Δc and the obtained P_{con}, the liquid-phase diffusion time constant τ_e can be directly obtained, as shown in formula (17).

$$\tau_e(t_{k+1}) = \frac{P_{con}.I(t)_k - \Delta c(t_k)}{\Delta c(t_{k+1}) - \Delta c(t_k)}.(t_{k+1}) - (t_k) \quad (17)$$

The identification results of LFP's battery parameters are shown in Table 2.

TABLE 2. Parameter identification results.

Parameter/Units	Value
y_0/-	0.2880
Q_p/C	3.2238×10^5
Q_n/C	2.3365×10^5
y_{ofs}/-	0.2011
P_{act}/(mol$^{0.5}$ s /m$^{1.5}$)	20115
τ_p/s	1
τ_n/s	32.8151
P_{con}/(mol/m^3/A)	11.9871
τ_e/s	38.3652
R_{ohm}/Ω	0.0064

The current excitation and voltage response in the parameter identification process are shown in Figure 3.

In order to verify the accuracy of model parameter identification, the constant current discharge experiment was performed. The comparison of voltage simulation curve and measured curve at 1C and 2C rate constant discharge is shown in Figure 4. The average error and of voltage and the capacity simulation error are shown in table 3.

According to the simulation error of voltage and capacity, SEM can well describe the behavior of the battery. Especially the capacity simulation error at 1C rate is only 0.42%.

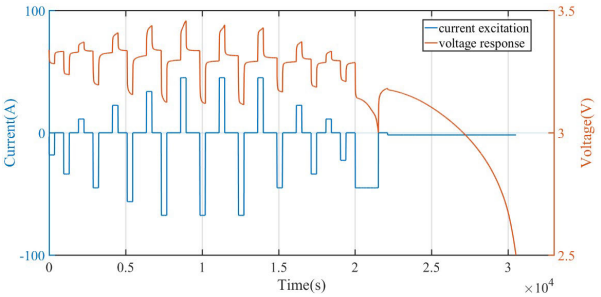

FIGURE 3. Current excitation and voltage response of parameter identification.

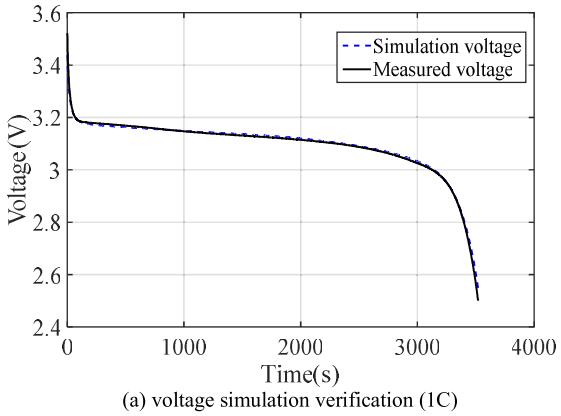

(a) voltage simulation verification (1C)

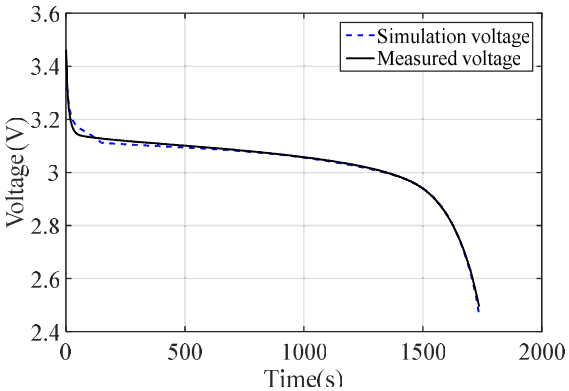

(b) voltage simulation verification (2C)

FIGURE 4. Comparison of measured voltage and simulated voltage.

TABLE 3. The simulation error of SEM.

current rate(-)	average voltage error (mV)	average capacity error (Ah)
1C	18.03	0.1875
2C	20.27	0.2625

Therefore, it is feasible to predict the RUL based on the SEM simulation.

IV. RUL PREDICTION BY INTEGRATING SIMPLIFIED ELECTRO-CHEMICAL MODEL TO THE PF FRAMEWORK

A. CYCLIC AGING EXPERIMENT

In order to investigate the relevance between the parameters in the SEM and battery aging process, a cyclic aging experiment was performed. In this paper, the 45Ah cylindrical

$LiFePO_4$ batteries were used to perform cyclic aging and parameter identification experiments. The battery test system is produced by Newware Co., Ltd, China.

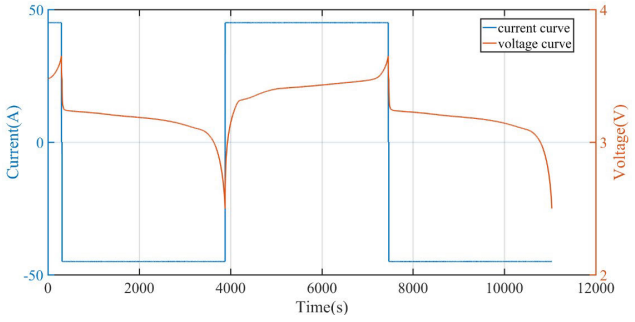

FIGURE 5. Current and voltage profiles in aging experiment.

The cyclic aging conditions consist of constant current charge and constant current discharge at 1C rate. Among them, the cut-off voltage of constant current charge is 3.65V, and the cut-off voltage of constant current discharge is 2.5V. There is a 10 seconds interval between constant current charge and discharge. Constant voltage charge was removed because it is time consuming. Parameter identification experiment was performed after every 20 aging cycles. Fig.5 shows one section of current and the terminal voltage accordingly in the repeated aging process. In order to avoid the influence of ambient temperature on the capacity, the cyclic aging experiment was performed in the incubator which maintains a constant temperature of 25 °C. The flow chart of the cyclic aging experiment is shown in Fig. 6. Before the cyclic aging experiment is performed, the parameters identification was performed first. Parameters identification experiment was performed after every 20 aging cycles. There is a 30 minutes interval between parameters identification test and cyclic aging test When the battery capacity decays to 80% of the initial capacity, which is 36Ah, the cycle aging experiment ends.

B. EXTRACTION OF HEALTH CHARACTERISTICS

There are 10 parameters with independent physical significance in the SEM. Parameters with strong correlation with capacity can be selected as health characteristics for RUL prediction. The correlation between model parameters and capacity is not completely linear from the results of the cyclic aging experiment. Spearman's correlation coefficient in statistics is not limited by the sample size, variable distribution and whether the data has continuity. Therefore, spearman's correlation coefficient (ρ) is used to screen health characteristics in this paper. The results of correlation analysis are shown in table 4.

The parameters y_{ofs}, Q_p, Q_n, P_{act}, R_{ohm}, and τ_{sn} are considered as HCs by criterion of "$|\rho| > 0.95$". Positive and negative ratio shift (y_{ofs}) increases exponentially with the number of cycles, which is caused by the shrinkage and shift of the positive and negative open circuit curves during

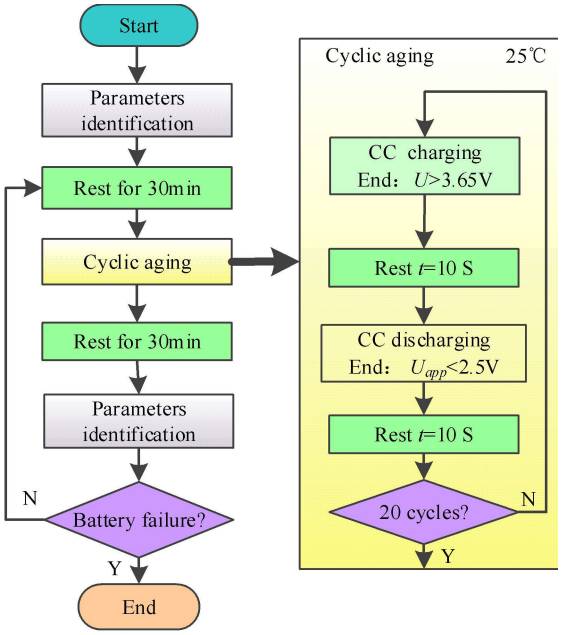

FIGURE 6. Cyclic aging experiment flow char.

TABLE 4. Correlation between SEM parameters and capacity.

Parameters	ρ value	Degree of relevance
y_0	0.6692	weak
y_{ofs}	-0.9736	strong
Q_p	0.9868	strong
Q_n	0.9868	strong
P_{act}	-0.9780	strong
P_{con}	-0.6659	weak
R_{ohm}	-0.9734	strong
τ_p	-	no
τ_n	-0.4824	weak
τ_e	-0.7231	weak

the battery aging process. Positive and negative capacity, Q_p and Q_n, degrade with the number of cycles that is caused by the loss of active material and the available lithium ion. The ohmic resistance, R_{ohm}, increase exponentially reflecting that the solid electrolyte interface (SEI) film on the surface of the active particles is constantly growing during the aging process. The reaction polarization coefficient, P_{act}, increase exponentially reflecting that the electrochemical reaction on the surface of the active material becomes more difficult with the aging of the battery.

According to the data of the cycle aging test and the parameter identification experiment, the relationship between

TABLE 5. Fittings of the HCs with the number of cycles.

Parameter	Fitting formula	Formula type	R^2
y_{ofs}	0.010355×exp(-0.01343×N)+0.1995	$a_1 \exp(b_1 N) + c_1$	0.9654
Q_p	-2807×exp(0.0113×N)+3.232×10^5	$a_2 \exp(b_2 N) + c_2$	0.9922
Q_n	-16.94×N +2.338×10^5	$a_3 N + b_3$	0.9787
R_{ohm}	0.07133×exp(0.01057×N)+4.985	$a_4 \exp(b_3 N) + c_4$	0.9686
P_{act}	7899×exp(0.007458×N)+1.114×10^4	$a_5 \exp(b_4 N) + c_5$	0.9579

each health characteristic and the number of cycles was fitted, and the fitting formula is shown in table 5.

C. RUL PREDICTION BASED ON PARTICLE FILTER

Particle Filter (PF) is an approximate Bayesian filtering algorithm based on Monte Carlo method, which is not restricted by the linear Gaussian problem. The core idea of PF is to use some discrete random sampling points to approximate the probability density function of the system random variables. The sample mean is used to replace the integral operation by sequence importance sampling, and then the minimum variance estimate of the state variable is obtained.

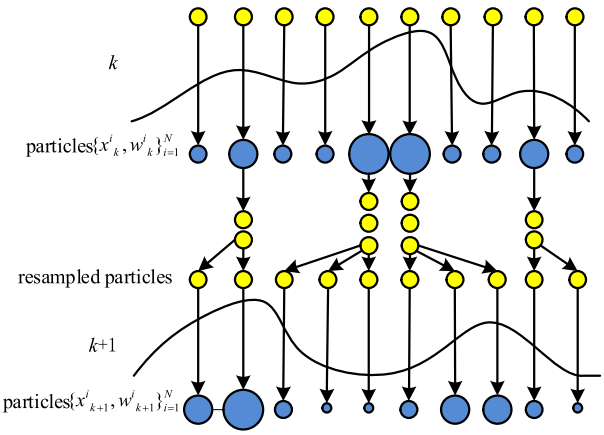

FIGURE 7. Schematic diagram of the PF algorithm.

The schematic diagram of the PF algorithm is shown in Fig.7. First, the initial particle set is generated according to the prior probability distribution of the system state quantity, and then it is weighted and recursively based on Bayesian theory to obtain the posterior probability distribution of the state quantity. Finally, the estimated value of the state quantity can be obtained combining with the Monte Carlo method. When the number of particles is infinite, the estimated value of particle filtering can infinitely approximate the optimal estimate, which is equivalent to the posterior probability density function [18]. Next, the RUL prediction framework based on PF algorithm is introduced. For comparison, the data-driven PF-based LIBs RUL prediction framework is first introduced. In reference [19], the relationship between the battery capacity model and the number of cycles is a double exponential function, such as formula (18), which is the observation equation in the PF.

$$Q_k = a_k \exp(b_k \cdot k) + c_k \exp(d_k \cdot k) + v_k \tag{18}$$

where Q_k is the capacity of battery, k is the cycle number, v_k is zero-mean Gaussian noise, parameters a_k, b_k, c_k, and d_k are state variables that constitute state vector $x_k = \{a_k, b_k, c_k, d_k\}^T$.

The update process of state variables can be expressed by the following Eq.(19), which is the state equation in PF.

$$\begin{cases} a_{k+1} = a_k + w_{a,k} \\ b_{k+1} = b_k + w_{b,k} \\ c_{k+1} = c_k + w_{c,k} \\ d_{k+1} = d_k + w_{d,k} \end{cases} \tag{19}$$

where, $w_{a,k}$, $w_{b,k}$, $w_{c,k}$, and $w_{d,k}$ are all zero-mean Gaussian noises.

As we can see, the state equation and the observation equation don't take battery's mechanism into consideration. Moreover, the initial value of the no physical meaning state variables can be randomly selected or obtained by data fitting.

In order to improve the RUL prediction accuracy and reliability, a new PF framework based on SEM simulation has been established. The state variables are health characteristics and form a vector, $x_k = \{y_{ofs,k}, Q_{p,k}, Q_{n,k}, R_{ohm,k}, P_{act,k}\}^T$.

According to table 5, the state equation can be concluded as Eq. (20).

$$\begin{pmatrix} y_{ofs,k+1} \\ Q_{p,k+1} \\ Q_{n,k+1} \\ R_{ohm,k+1} \\ P_{act,k+1} \end{pmatrix} = \begin{pmatrix} e^{b_1} & 0 & 0 & 0 & 0 \\ 0 & e^{b_2} & 0 & 0 & 0 \\ 0 & 0 & 1 & 0 & 0 \\ 0 & 0 & 0 & e^{b_4} & 0 \\ 0 & 0 & 0 & 0 & e^{b_5} \end{pmatrix} \begin{pmatrix} y_{ofs,k} \\ Q_{p,k} \\ Q_{n,k} \\ R_{ohm,k} \\ P_{act,k} \end{pmatrix} + \begin{pmatrix} c_1(1-e^{b_1}) \\ c_2(1-e^{b_2}) \\ a_3 \\ c_4(1-e^{b_4}) \\ c_5(1-e^{b_5}) \end{pmatrix} + \begin{pmatrix} w_{ofs,k} \\ w_{p,k} \\ w_{n,k} \\ w_{ohm,k} \\ w_{act,k} \end{pmatrix} \tag{20}$$

Coefficients a_3, b_1, b_2, b_4, b_5, c_1, c_2, c_4, and c_5 have been obtained by Least Square fitting method in table 5. Vector

$w_k = \left[w_{\varepsilon_{\mathrm{p}},k}, w_{a_{\mathrm{sp}},k}, w_{a_{\mathrm{sn}},k}, w_{i_{0\mathrm{p}},k}, w_{i_{0\mathrm{n}},k}\right]^{\mathrm{T}}$ is the Gaussian process noise vector and k is the cycle number.

The observation equation in RUL prediction relates state variables with battery's capacity and is presented in Eq.(21)

$$Q_k = f(y_{\mathrm{ofs},k}, Q_{\mathrm{p},k}, Q_{\mathrm{n},k}, R_{\mathrm{ohm},k}, P_{\mathrm{act},k}) + v_k \qquad (21)$$

where f denotes the process of simulating battery's capacity using the SEM and function v_k is the Gaussian observation noise.

The capacity simulation can be carried out as such: a full charged battery is discharged at current rate of 1C until the voltage reaches 2.5V, and the discharging time can be obtained. Then the product of discharge current and discharge time is the estimation of capacity. Other parameters used in the simulation are considered as the average of previous identification results. A new PF framework for RUL prediction is established by combining SEM simulation. The state variables have explicit physical meaning and the observation equation simulates the battery capacity, which fully considered the mechanism behind state variables.

D. ANALYSIS OF RUL PREDICTION RESULTS

During the RUL prediction process, the battery life end point is set to the number of cycle when the capacity declines to 80% of the rated capacity. The capacity data is divided into training data and testing data. Both SEM-based and data-driven-based PF algorithm are used when the beginning of prediction (BOP) is the 80th cycle and the 160th cycle respectively.

The settings of the two PF algorithms are as follows: The number of particles was set 500 and the residual resampling was used. The process noise was $w_k = [1 \times 10^{-4}, 1 \times 10^{-4}, 1 \times 10^{-4}, 1 \times 10^{-4}]^{\mathrm{T}}$, while the observation noise was $v_k = 1 \times 10^{-3}$. What's more in data-driven-based PF algorithm. Unlike data-driven PF algorithm, the process noise was $w_k = [1 \times 10^{-5}, 1 \times 10^{4}, 1 \times 10^{3}, 1 \times 10^{-6}, 1 \times 10^{4}]^{\mathrm{T}}$, while the observation noise was $v_k = 1 \times 10^{-1}$ in SEM-based PF algorithm.

1) PREDICTION WITH BOP = 80

Firstly, data-driven-based PF framework was used to predict the LIBs RUL. The capacity data of the first 80 cycles is used to train the PF algorithm. The RUL prediction result and its corresponding PDF are shown in Fig.8 (a), (b). The capacity and model parameters of the previous 80 cycles are training data for SEM-based PF algorithm. Similarly, the RUL prediction result of SEM-based PF algorithm and its corresponding PDF are shown in Fig.8 (c), (d).

According to the data of the cycle aging experiment, the cycle life of the battery is 250 cycles. The capacity of the previous 80 cycles is training data, and the cycle life of the battery predicted by the data-driven PF algorithm is 220 cycles. The predicted value differs from the actual value by 30 cycles.

The cycle life of the battery predicted by the SEM-based PF algorithm is 238 cycles. The predicted value differs from the actual value by 12 cycles. From the prediction results, the SEM-based particle filter algorithm considering the battery aging mechanism has better performance. Compared with data-driven RUL prediction algorithm, the prediction of LIBs RUL is closer to reality after considering the aging mechanism.

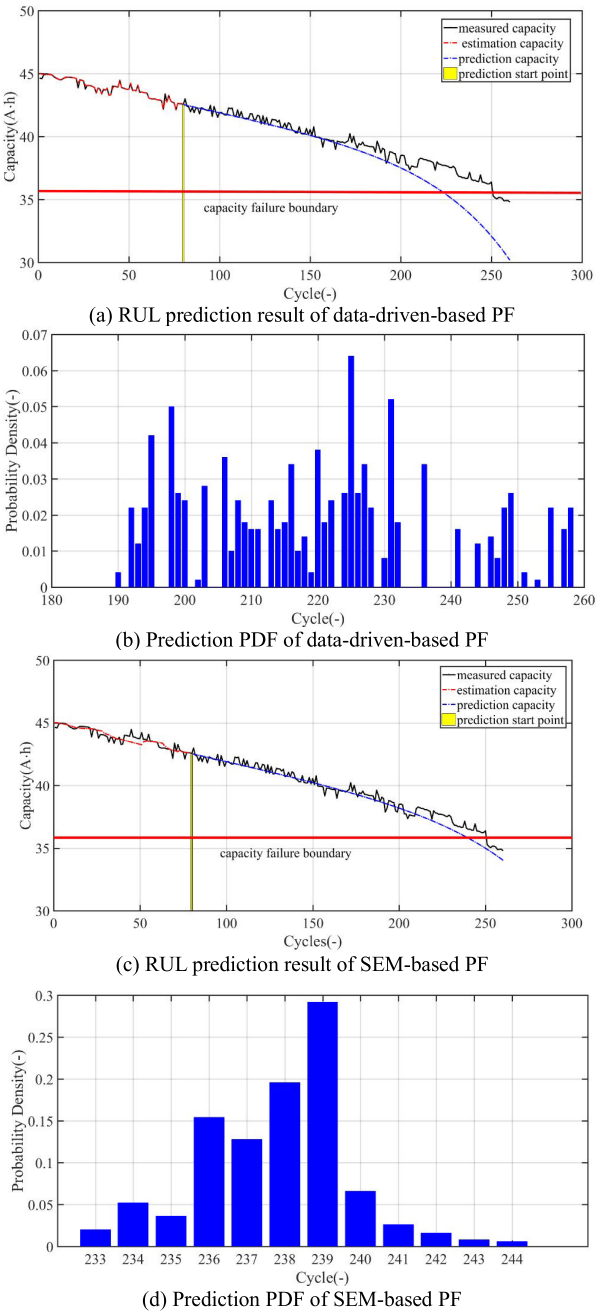

(a) RUL prediction result of data-driven-based PF

(b) Prediction PDF of data-driven-based PF

(c) RUL prediction result of SEM-based PF

(d) Prediction PDF of SEM-based PF

FIGURE 8. RUL prediction result of data-driven-based PF framework and SEM-based PF framework (BOP = 80).

2) PREDICTION WITH BOP = 160

The capacity data of the first 160 cycles was used to train the data-driven-based PF algorithm. The RUL prediction results and its corresponding PDF are shown in Fig.9 (a), (b).

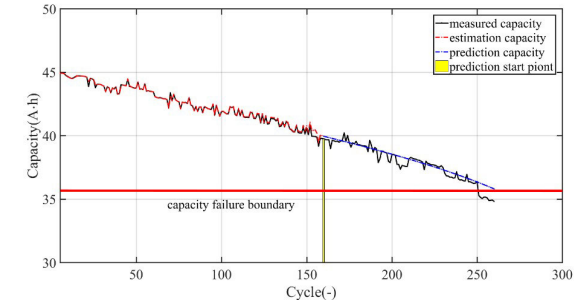

(a) RUL prediction result of data-driven-based PF

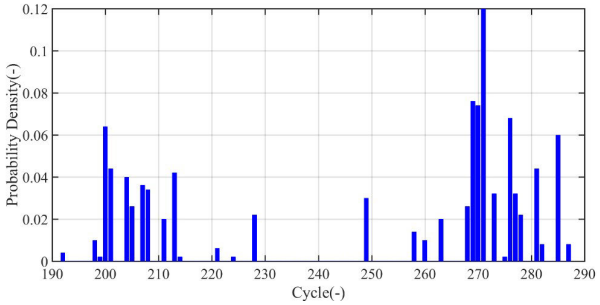

(b) Prediction PDF of data-driven-based PF

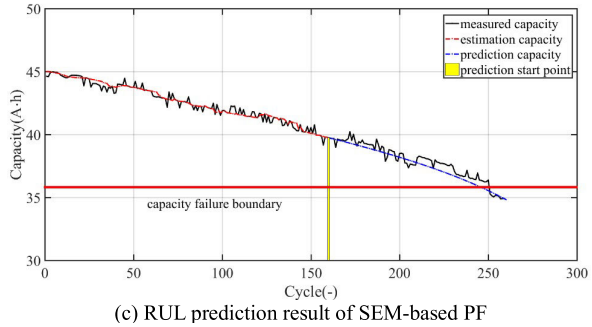

(c) RUL prediction result of SEM-based PF

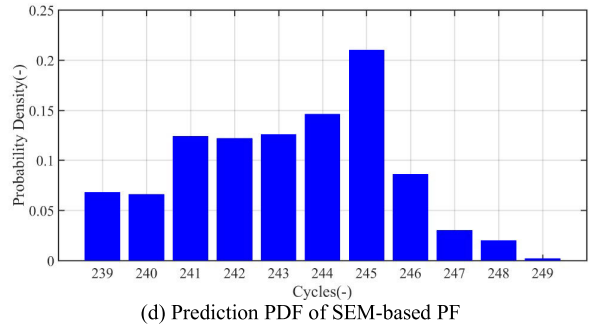

(d) Prediction PDF of SEM-based PF

FIGURE 9. **RUL prediction result of data-driven-based PF framework and SEM-based PF framework (BOP = 160).**

The capacity and model parameters of the previous 160 cycles are training data for SEM-based PF algorithm. Similarly, the RUL prediction result of SEM-based PF algorithm and its corresponding PDF are shown in Fig.9 (c), (d).

The cycle life of the battery predicted by the data-driven PF algorithm is 270 cycles. The predicted value differs from the actual value by 20 cycles. Compared with Fig. 8 (a), the prediction performance of data-driven PF algorithm does not significantly improve with the increase of training data. Since the latter segment of the training data is relatively flat, the number of cycles predicted by the PF algorithm changes from 220 to 270, which exceeds the actual value. It can be seen that the data-driven PF algorithm is affected by the characteristics of the training data.

TABLE 6. **Description of the SEM governing equation.**

Physics	Model description
Terminal voltage	$U_{app}(t) = E_{ocv}(t) - \eta_{con}(t) - \eta_{act}(t) - \eta_{ohm}(t)$
Basic working process	$y_{avg} = y_0 + (1 - SOC)Q_{all} / Q_p$
	$x_{avg} = \left(1 - y_{ofs} - y_{avg}\right) Q_p / Q_n$
	$E_{ocv}^{ref}(t) = U_p(y_{surf}) - U_n(x_{surf})$
Solid phase diffusion	$\Delta y'(t_{k+1}) = \Delta y'(t_k) + \frac{1}{\tau_p^s} \cdot \left[\frac{12}{7} \frac{\tau_p}{Q_p} \cdot I(t_k) - \Delta y'(t_k) \right] \cdot (t_{k+1} - t_k)$
	$\Delta x'(t_{k+1}) = \Delta x'(t_k) + \frac{1}{\tau_n^s} \cdot \left[\frac{12}{7} \frac{\tau_n}{Q_n} \cdot I(t_k) - \Delta x'(t_k) \right] \cdot (t_{k+1} - t_k)$
	$\Delta y(t) = \Delta y'(t) + \frac{2}{7} \frac{\tau_p}{Q_p} I(t)$
	$\Delta x(t) = \Delta x'(t) + \frac{2}{7} \frac{\tau_n}{Q_n} I(t)$
Liquid phase diffusion	$\eta_{con}(t) = \frac{2RT(t)}{F} \left(1 - t_+\right) \cdot \left(\ln \frac{c_0 + \Delta c}{c_0 - \Delta c} \right)$
	$\Delta c(t) = P_{con} \left(1 - e^{-t/\tau_c}\right) I(t)$
Reaction polarization	$\eta_{act}(t) = \frac{2RT(t)}{F} \left[\ln(\sqrt{m_n^2(t) + 1} + m_n(t)) - \ln(\sqrt{m_p^2(t) + 1} + m_p(t)) \right]$
	$m_p(t) = \frac{1}{6 \cdot Q_p \cdot c_0^{0.5}} \cdot \frac{1}{\left(1 - y_{surf}\right)^{0.5} \left(y_{surf}\right)^{0.5}} \cdot P_{act} \cdot I(t)$
	$m_n(t) = \frac{1}{6 \cdot Q_n \cdot c_0^{0.5}} \cdot \frac{1}{\left(1 - x_{surf}\right)^{0.5} \left(x_{surf}\right)^{0.5}} \cdot P_{act} \cdot I(t)$
Ohmic polarization	$\eta_{ohm} = R_{ohm} \cdot I$

The cycle life of the battery predicted by the SEM-based PF algorithm is 245 cycles. The predicted value differs from the actual value by 5 cycles. Compared with Fig. 8 (c), as the training data increases, the performance of the RUL prediction improves as well. Under the premise of considering the battery mechanism, the increase in training data means that more aging information can be used, so the predicted performance will become better. Compared with the data-driven PF algorithm, SEM-based PF has better prediction performance and better stability.

V. CONCLUSION

This paper realizes a new electrochemical-model-based PF framework for LIB RUL prediction in which the mechanisms of battery are fully considered. The merits of this paper are:

The parameters of a simplified electrochemical model are selected as battery health characteristics, which can be

identified by applying characteristic excitation currents to the battery. The change trend of these health characteristics with the aging of the battery can be obtained by fitting an exponential function or a linear function.

The state variables of the new PF algorithm are selected from battery's health characteristics rather than meaningless fitting coefficients. The new state equation comes from the trends of health characteristics. The observation equation is essentially the simulation of battery's capacity which makes the RUL prediction more robust by introducing the mechanism of battery.

The methodology fills the research gap between battery mechanism and data-driven PF RUL prediction and provides an option for high quality RUL prediction applications.

APPENDIX

See Table 6.

REFERENCES

[1] S. Zhu, C. Hu, Y. Xu, Y. Jin, and J. Shui, "Performance improvement of lithium-ion battery by pulse current," *J. Energy Chem.*, vol. 46, pp. 208–214, Jul. 2020.
[2] C. Lyu, Q. Lai, T. Ge, H. Yu, L. Wang, and N. Ma, "A lead-acid battery's remaining useful life prediction by using electrochemical model in the particle filtering framework," *Energy*, vol. 120, pp. 975–984, Feb. 2017.
[3] A. Nuhic, T. Terzimehic, T. Soczka-Guth, M. Buchholz, and K. Dietmayer, "Health diagnosis and remaining useful life prognostics of lithium-ion batteries using data-driven methods," *J. Power Sources*, vol. 239, pp. 680–688, Oct. 2013.
[4] T. Qin, S. Zeng, and J. Guo, "Robust prognostics for state of health estimation of lithium-ion batteries based on an improved PSO–SVR model," *Microelectron. Rel.*, vol. 55, nos. 9–10, pp. 1280–1284, Aug. 2015.
[5] L. Li, P. Wang, K. H. Chao, Y. Zhou, and Y. Xie, "Remaining useful life prediction for lithium-ion batteries based on Gaussian processes mixture," *PLoS ONE*, vol. 11, no. 9, pp. 1–13, 2016.
[6] B. Long, W. Xian, L. Jiang, and Z. Liu, "An improved autoregressive model by particle swarm optimization for prognostics of lithium-ion batteries," *Microelectron. Rel.*, vol. 53, no. 6, pp. 821–831, Jun. 2013.
[7] G. Ma, Y. Zhang, C. Cheng, B. Zhou, P. Hu, and Y. Yuan, "Remaining useful life prediction of lithium-ion batteries based on false nearest neighbors and a hybrid neural network," *Appl. Energy*, vol. 253, Nov. 2019, Art. no. 113626.
[8] Y. Zhang, R. Xiong, H. He, and M. G. Pecht, "Long short-term memory recurrent neural network for remaining useful life prediction of lithium-ion batteries," *IEEE Trans. Veh. Technol.*, vol. 67, no. 7, pp. 5695–5705, Jul. 2018.
[9] X. Hu, S. E. Li, Z. Jia, and B. Egardt, "Enhanced sample entropy-based health management of li-ion battery for electrified vehicles," *Energy*, vol. 64, pp. 953–960, Jan. 2014.
[10] Z. Guo, X. Qiu, G. Hou, B. Y. Liaw, and C. Zhang, "State of health estimation for lithium ion batteries based on charging curves," *J. Power Sources*, vol. 249, pp. 457–462, Mar. 2014.
[11] Y. Li, M. Abdel-Monem, R. Gopalakrishnan, M. Berecibar, E. Nanini-Maury, N. Omar, P. van den Bossche, and J. Van Mierlo, "A quick on-line state of health estimation method for li-ion battery with incremental capacity curves processed by Gaussian filter," *J. Power Sources*, vol. 373, pp. 40–53, Jan. 2018.
[12] K. Maher and R. Yazami, "A study of lithium ion batteries cycle aging by thermodynamics techniques," *J. Power Sources*, vol. 247, pp. 527–533, Feb. 2014.
[13] S. E. Li, B. Wang, H. Peng, and X. Hu, "An electrochemistry-based impedance model for lithium-ion batteries," *J. Power Sources*, vol. 258, pp. 9–18, Jul. 2014.
[14] X. Zheng and H. Fang, "An integrated unscented Kalman filter and relevance vector regression approach for lithium-ion battery remaining useful life and short-term capacity prediction," *Rel. Eng. Syst. Saf.*, vol. 144, pp. 74–82, Dec. 2015.
[15] Q. Miao, L. Xie, H. Cui, W. Liang, and M. Pecht, "Remaining useful life prediction of lithium-ion battery with unscented particle filter technique," *Microelectron. Rel.*, vol. 53, no. 6, pp. 805–810, Jun. 2013.
[16] B. Saha, K. Goebel, and J. Christophersen, "Comparison of prognostic algorithms for estimating remaining useful life of batteries," *Trans. Inst. Meas. Control*, vol. 31, nos. 3–4, pp. 293–308, Jun. 2009.
[17] C. Lyu, Y. Song, J. Zheng, W. Luo, G. Hinds, J. Li, and L. Wang, "*In situ* monitoring of lithium-ion battery degradation using an electrochemical model," *Appl. Energy*, vol. 250, pp. 685–696, Sep. 2019.
[18] A. T. Cemgil, "A tutorial introduction to Monte Carlo methods, Markov chain Monte Carlo and particle filtering," in *Academic Press Library in Signal Processing*, vol. 1. 2014, pp. 1065–1114.
[19] Y. Chang, H. Fang, and Y. Zhang, "A new hybrid method for the prediction of the remaining useful life of a lithium-ion battery," *Appl. Energy*, vol. 206, pp. 1564–1578, Nov. 2017.